10) Shibuya M, et al. Proteomic & Transcriptomic Analyses of Retinal Pigment Epithelial Cells Exposed to REF-1/TFPI-2, a Growth Promoting Factor. Invest Ophthal Vis Sci 2007;48:516-521.

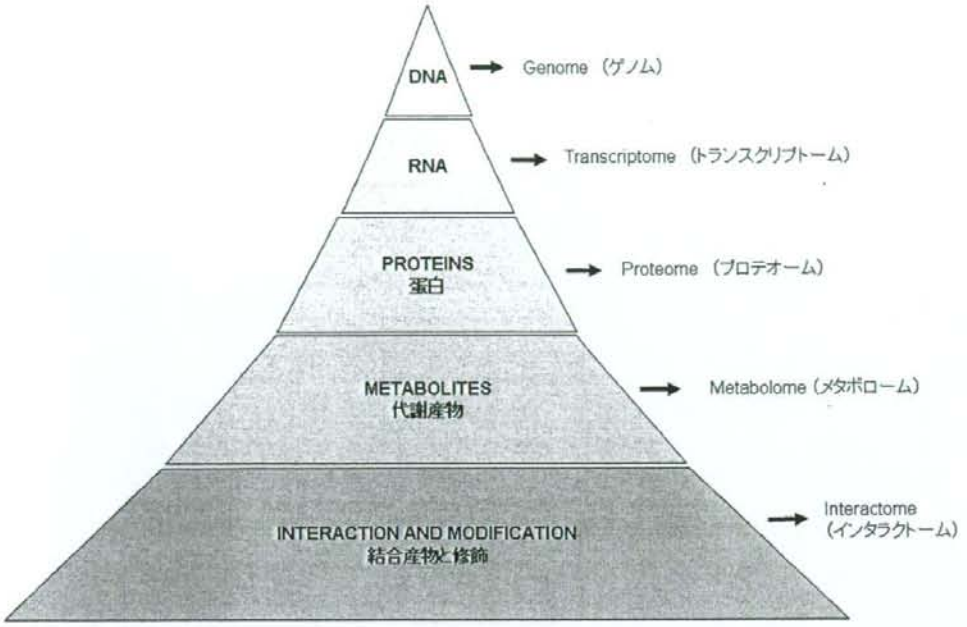

図1　生命現象の研究を総称してフェノミックスという。

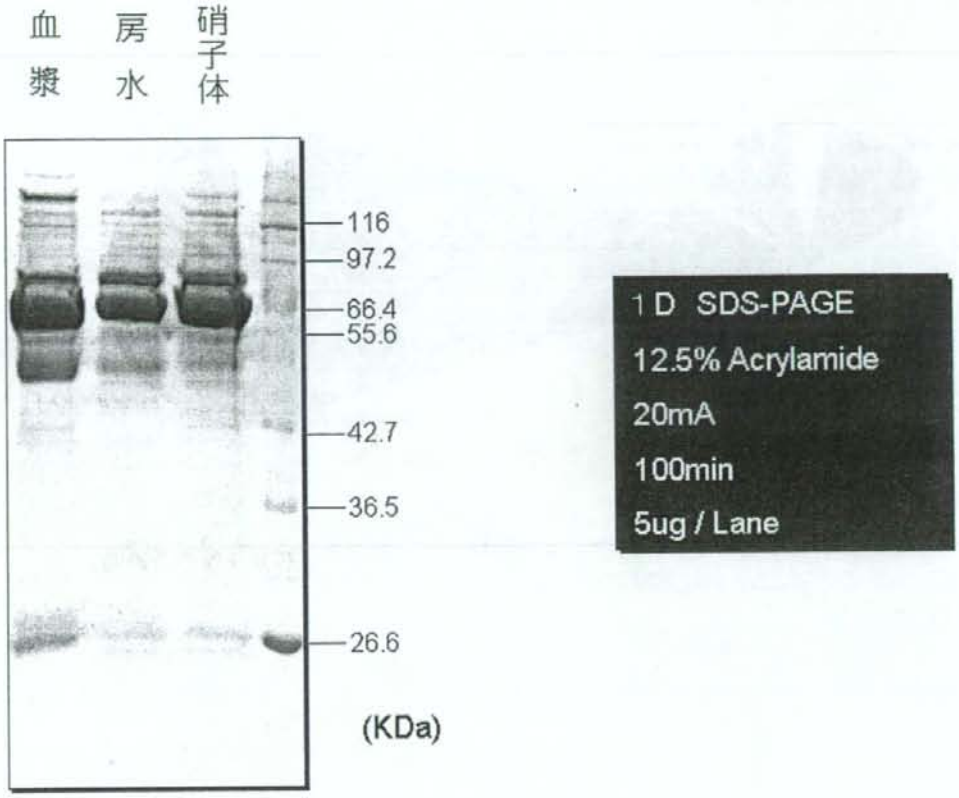

図2　一次元電気泳動による血漿、房水、硝子体の分画。

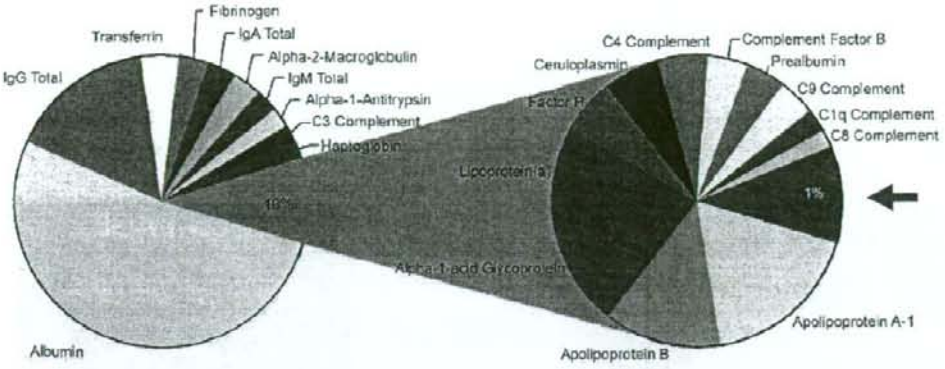

図３　血漿に含まれる蛋白とその割合。２２種類のタンパク質が９９％を占める。

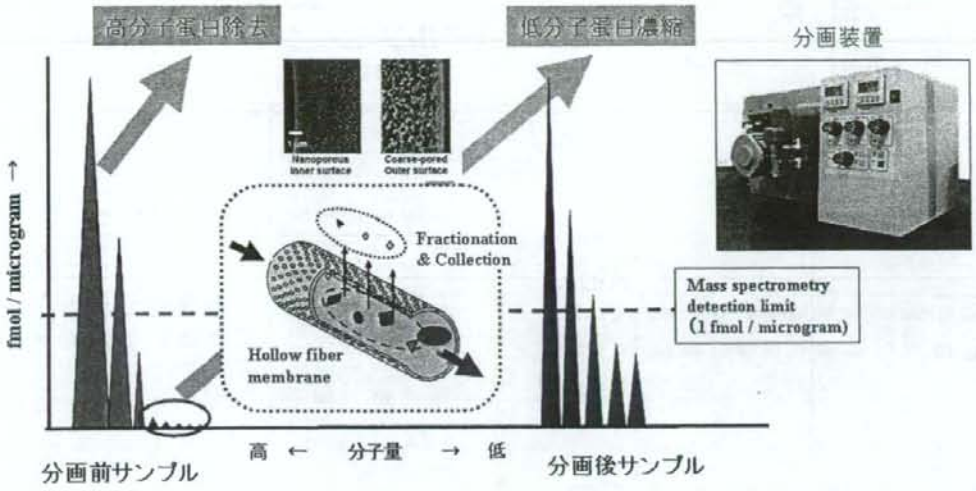

図４　中空紙を使った蛋白分画装置（東レ株式会社製造）による低分子量蛋白の濃縮

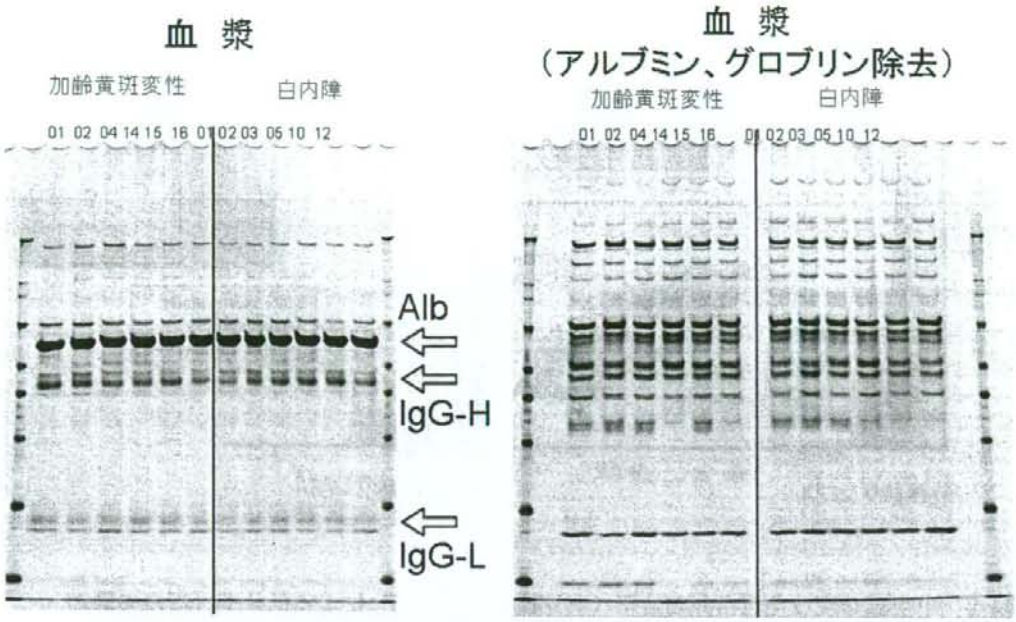

図５　血漿プロテオーム解析。加齢黄斑変性と白内障患者の血漿を一次元電気泳動によって分画した。

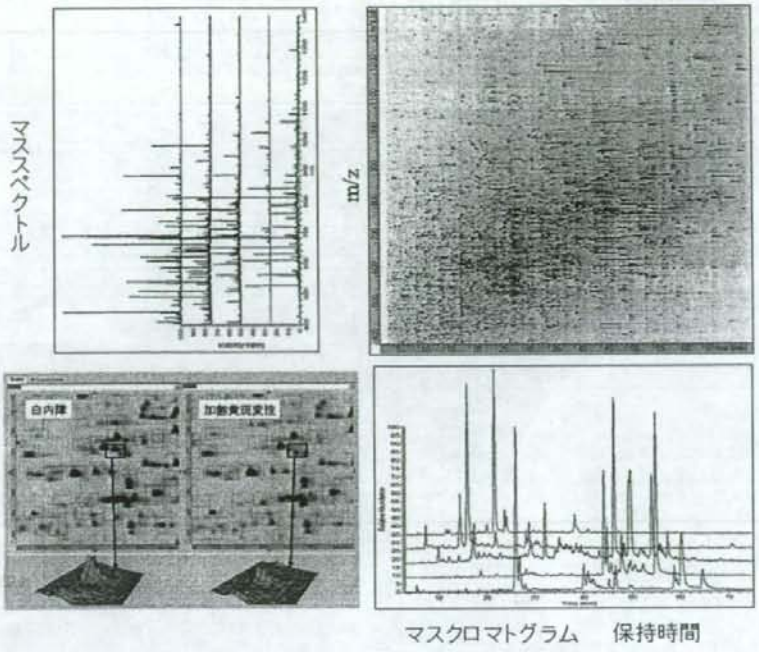

図6　質量分析計のマススペクトルとマスクロマトグラムによる擬似的二次元表示。蛋白量はスポットの濃さとして表示される。

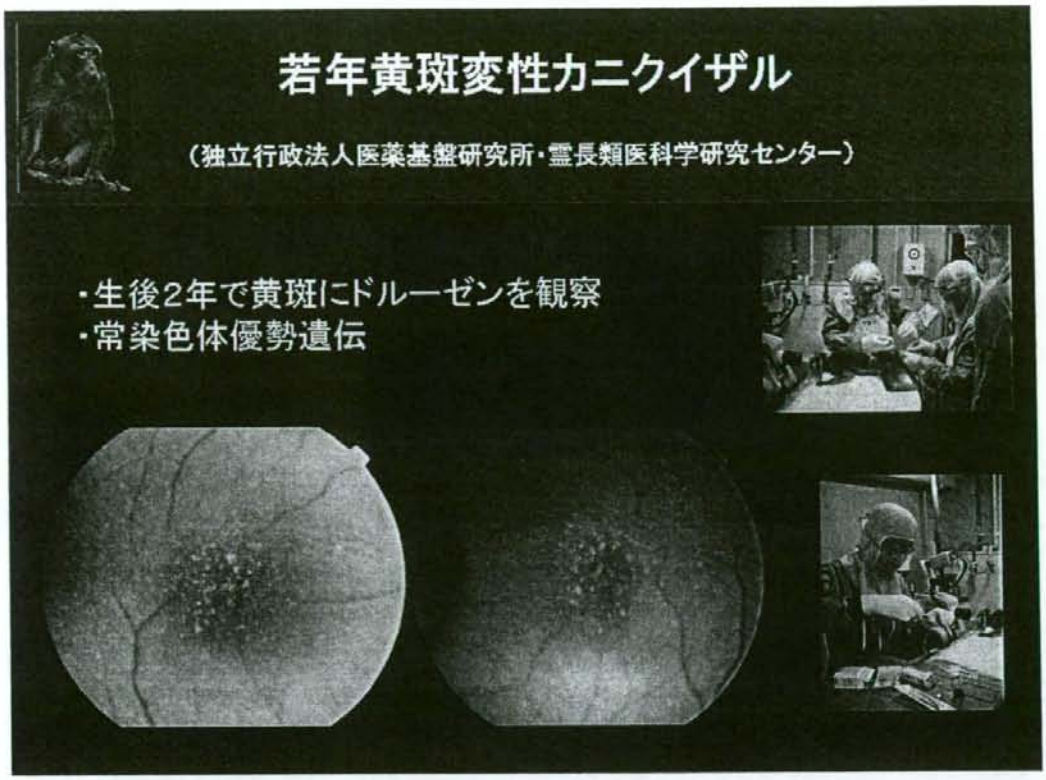

図７　独立行政法人医薬基盤研究所霊長類医科学研究センターで発見された若年性黄斑変性カニクイザルの眼底写真

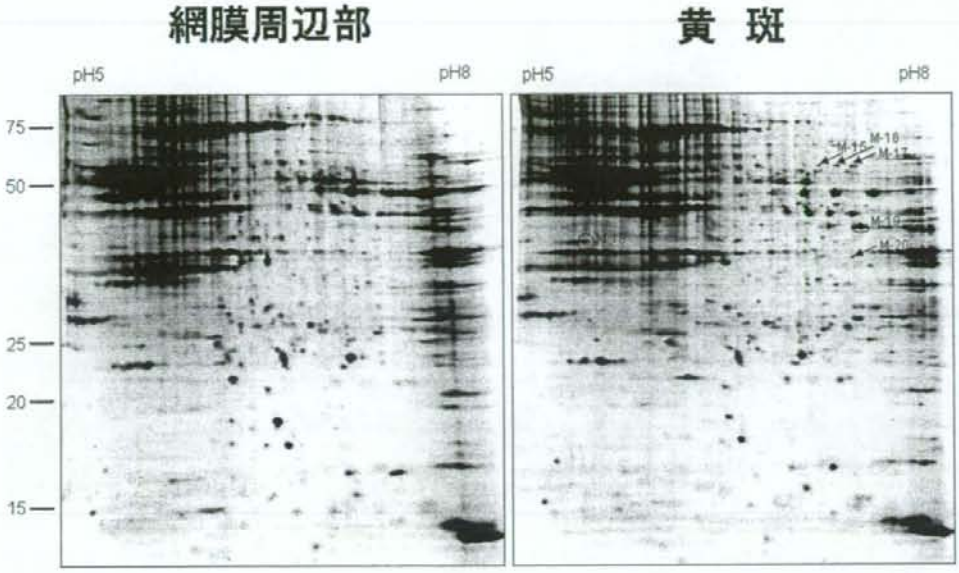

図８　黄斑のプロテオーム解析。網膜周辺部と黄斑の二次元電気泳動パターン。黄斑に特異的な蛋白が発見された（矢印）。

Discovery of Potential Sorbitol Dehydrogenase Inhibitors from Virtual Screening

Connie Darmanin[a], Takeshi Iwata[b], Deborah A. Carper[c] and Ossama El-Kabbani[a,*]

[a]*Department of Medicinal Chemistry, Victorian College of Pharmacy, Monash University (Parkville Campus), Parkville, Victoria 3052, Australia;* [b]*National Institute of Sensory Organs, National Hospital Organization Tokyo Medical Center, 2-5-1 Higashigaoka, Meguro-ku, Tokyo 152-8902, Japan;* [c]*National Eye Institute, NIH, Bethesda MD 20892, USA*

Abstract: Sorbitol dehydrogenase (SDH) is the second enzyme in the polyol pathway of glucose metabolism and is a possible target for the treatment of the complications of diabetes. In this study the molecular modelling program DOCK was used to analyse 249,071 compounds from the National Cancer Institute Database and predict those with high affinity for SDH. From a total of 21 tested the 7 compounds including flavin adenine dinucleotide disodium hydrate, (+)-Amethopterin, 3-hydroxy-2-napthoic(2-hydroxybenzylidene) hydrazide, folic acid, N-2,4-dinitrophenyl-L-cysteic acid, Vanillin azine and 1H-indole-2,3-dione,5-bromo-6-nitro-1-(2,3,4-tri-O-acetyl-α-L-arabinopyranosyl)-(9Cl), were shown to inhibit SDH and displayed IC_{50} values of 0.192 μM, 1.1 μM, 1.2 μM, 4.5 μM, 5.3 μM, 7 μM and 28 μM, respectively. These compounds may aid the design of pharmaceutical agents for the treatment of diabetes complications.

INTRODUCTION

Sorbitol dehydrogenase (SDH) is expressed in all mammalian tissues, including the brain, lens, erythrocytes and liver [1,2]. The enzyme has attracted considerable interest owing to its implication in the development of diabetic complications such as cataracts, neuropathy, retinopathy and nephropathy [3]. The structure of human SDH with and without the bound inhibitor 2-hydroxymethyl-4-(4′-*N*,*N*-dimethylaminosulfonyl-1-piperazino) pyrimidine (SDI-158) has been recently published [4]. The overall structure was found to be similar to those of rat SDH [5], NADPH-dependant whitefly ketose reductase [6], and human liver ADH [7]. The catalytic zinc atom was coordinated by His69, Cys44, Glu70 and a water molecule (tetra-coordination) in both the apo- and holoenzyme structures. In the ternary structure, penta-coordination of the zinc occurred with simultaneous interactions with the N1 nitrogen and O30 oxygen of SDI-158 and dissociation of Glu70.

Prior to the year 2000, only one known *in vivo* prototype SDH inhibitor (SDI), SDI-158, was reported in the literature. Since then the synthesis of pyridine derivatives, which had a 4′-*N*,*N*-dimethylaminosulfonyl-1-piperazino group at the 4-position and various functionalities, including hydrogen, CH_2OH, CHO, $CONH_2$ and CN, at the 2-position were reported [8]. The inhibitory activities of these derivatives were investigated to determine their potential as novel SDIs. The pyridine group was selected as a template because of its similarity to the pyrimidine group in SDI-158 and the various functionalities at 2-position of the pyridine ring were then used to establish structure-activity relationships. However, when tested against SDH, these compounds were shown to be less effective inhibitors than SDI-158, hence it was concluded that the pyrimidine moiety is important for the active site interactions. New SDH inhibitors were synthesised by replacing the dimethylaminosulfonyl group in SDI-158 with a variety of heterocycles and found to inhibit SDH with the most potent IC_{50} value equal to 10 nM [9]. Based on these findings, the dimethylaminosulfonyl group was targeted and an SDI with an IC_{50} value of 4 nM that has very good drug-like properties, including a long plasma half-life, was recently reported [10].

The program DOCK (version 4.0) [11] is used to orient small molecules into potential binding sites of proteins by matching the receptor pocket to the ligand atoms or surfaces. An energy score is given based on the complementarity between the ligand and the receptor, i.e. geometry as well as overall chemical complementarity and steric fit. The docking methodology used in this study has been described in detail in the literature [12,13]. In this case, the crystal structure of the human SDH holoenzyme [4] together with the DOCK program were used to search the NCI database [14] for possible compounds that may inhibit SDH or serve as new templates for further inhibitor development.

NCI DATABASE SEARCH

The coordinates of the human SDH/NAD^+ complex (PDB code: 1PL8) and the NCI database (249,071 compounds) were used to search for potential inhibitors or drug templates of SDH. The DOCK program [11] read 234,244 compounds, of which 230,747 compounds were docked successfully. A total number of 3,497 compounds were skipped due to the chemical and physical filters utilised by the program. This includes ignoring compounds that contain heavy atoms such as Zn, Al, Au or Ag or compounds that had too many or incorrectly assigned rotatable bonds. 15,756 compounds (6.3% of the database) were found to be chemically toxic (i.e. containing atoms such as Pt, Hg, Pu, Cr or Ir) and were also excluded from the database. Hydrogen atoms, partial

*Address correspondence to this author at the Department of Medicinal Chemistry, Victorian College of Pharmacy, Monash University (Parkville Campus), Parkville, Victoria 3052, Australia; Tel: +61 3 9903 9691; Fax: +61 3 9903 9582; E-mail: ossama.el-kabbani@vcp.monash.edu.au

1573-4064/06 $50.00+.00

charges, atomic potentials and bond orders for the complexes were assigned using the automatic procedures within the InsightII 2.1 package (Biosym Technologies Inc., San Diego, CA). Arginine, lysine, aspartate and glutamate amino acids were charged while the histidines were uncharged, with hydrogen atoms fixed at the Nε2. The Zn atom present in the active site of SDH was charged (2+). Using the program Concord the compounds were downloaded from the NCI database without altering their ionization states. Based on the SDH/SDI structure, a box was used to define the active site and included the Zn atom and Zn binding ligands. The docked compounds were restricted to the specified box. The top-ranked 3,000 compounds were checked for commercial availability using the NCI database website (www.cactus.nci.nih.gov) and only those compounds that were available were analysed thoroughly for their interactions with the active-site residues and Zn atom using the molecular modelling program InsightII (Biosym Technologies, San Diego, CA, USA). Compounds that had good interactions were then chosen for IC_{50} measurements as described below.

SDH EXPRESSION AND PURIFICATION

The coding region of human SDH (SORD) was isolated from the liver cDNA library, inserted into a prokaryotic expression vector (pET23 (+) Novagen, Madison, WI, USA) and transformed into *E. coli* BL21 (DE3) (Novagen) [15]. Briefly, SDH was purified from the supernatant by ammonium sulfate precipitation, anion exchange chromatography and affinity chromatography following established procedures [16]. The concentration, purity and enzymatic activity of SDH were examined at each step.

INHIBITORY ASSAY FOR SDH

Enzyme activity was determined using a Shimadzu UV-vis spectrophotometer (model UV160A) by following the increase in absorbance of NADH at 340 nm. SDH was tested for compound inhibition using compound stocks made up in 50% DMSO. The reaction was carried out with a 1 ml assay sample containing 42 mM glycine buffer pH 9.9, 9.9 mM D-sorbitol and 0.5 mM β-NAD^+ and different concentrations of compounds. Initially, the buffer and water were equilibrated to a constant temperature of 25° C in a hot water bath and a final concentration of DMSO in the assay not exceeding 2% was used. The reaction was commenced by addition of the substrate. One milli-unit (mU) of activity was defined as the amount of enzyme needed to oxidise 1 milli-mole of substrate per minute under initial velocity conditions at room temperature (20° C).

The DOCK program results suggested 21 compounds that may potentially inhibit SDH. These compounds were purchased and after the initial testings 7 compounds were found to be active. The active compounds included flavin adenine dinucleotide disodium hydrate, (+)-Amethopterin, 3-hydroxy-2-napthoic(2-hydroxybenzylidene) hydrazide, folic acid, N-2,4-dinitrophenyl-L-cysteic acid, Vanillin azine and 1H-indole-2,3-dione,5-bromo-6-nitro-1-(2,3,4-tri-O-acetyl-α-L-arabinopyranosyl)-(9Cl). The corresponding IC_{50} values were 0.192 μM, 1.1 M, 1.2 μM, 4.5 μM, 5.3 μM, 7 μM and 28 μM, respectively. The molecular formulae and chemical structures of the 7 active compounds are shown in Table **1**. For comparison and validation of the inhibitory assay the IC_{50} value of SDI-158 was also determined and was found to be in agreement with the published value [8]. In addition, SDI-158 was docked into the active site of SDH and the resulting orientation was found to be similar to that observed in the crystal structure of the ternary complex [4]. The most potent compound, with an IC_{50} value of 0.192 μM and 5.2-fold greater potency than SDI-158, is flavin adenine dinucleotide disodium hydrate. 1H-indole-2,3-dione,5-bromo-6-nitro-1-(2,3,4-tri-O-acetyl-α-L-arabinopyranosyl)-(9Cl) was the least potent with a 28-fold less potency compared to SDI-158.

While previous studies on SDIs were focused on the design and synthesis of analogues for SDI-158 [9-12], our study revealed novel classes of potential inhibitors with *in vitro* potencies in the micro molar range. The new compounds include a ring system, which seems to be a pre-requisite for SDH inhibitors and bind to a hydrophobic portion of the active site. Additionally, hydroxyls, sulfonic or nitro functional groups interacted with the polar residues and the catalytic zinc atom. Vanillin azine and 3-hydroxy-2-napthoic(2-hydroxybenzylidene) hydrazide have comparable structures including hydroxyl groups and benzyl rings, while (+)-Amethopterin is an analogue of folic acid. The proposed interactions between the most active compound (flavin adenine dinucleotide disodium hydrate) and the active site residues of SDH are shown in Fig. **1**.

Similar to SDI-158 [4], the potencies of the compounds *in vitro* are likely due to their interactions with the catalytic zinc. Additional interactions may include the stacking against the nicotinamide ring of NAD^+, the numerous van der Waals contacts and a small number of H-bonds between the compounds and the protein. The proposed models suggest that flavin adenine dinucleotide is coordinated to the zinc atom by oxygen and nitrogen atoms (1.8 Å and 1.9 Å, respectively) from the flavin ring which π-stacks against the nicotinamide ring of NAD^+ (Fig. 1). (+)-Amethopterin is H-bonded to His49 (3.0 Å) and Thr121 (2.9 Å). The zinc atom is likely coordinated by nitrogen atoms of the diaminopteridin ring (3.2 Å and 3.9 Å). In case of the 3-hydroxy-2-napthoic(2-hydroxybenzylidene) hydrazide the zinc atom may be coordinated by a nitrogen atom from the 2-hydroxybenzylidene moiety (2.7 Å). Folic acid is H-bonded to Ser46 (3.7 Å), Thr121 (3.1 Å), Glu155 (2.8 Å) and Ser276 (2.3 Å), and may coordinate to the zinc atom through two nitrogens from its 4-pteridinol ring (3.2 Å and 3.8 Å). N-2,4-Dinitrophenyl-L-cysteic acid is likely coordinated through its sulfomethyl oxygen to the zinc atom (2.4 Å). Vanillin azine forms an H-bond with Thr121 (3.0 Å) and may coordinate to the zinc atom through an imine nitrogen (2.4 Å). In the case of 1H-indole-2,3-dione,5-bromo-6-nitro-1-(2,3,4-tri-O-acetyl-α-L-arabinopyranosyl)-(9Cl), the zinc atom is likely coordinated by an ester oxygen (2.3 Å).

This was the first study on the discovery of potential SDH inhibitors from virtual screening and resulted in a 33% success rate. From a total of 21 compounds tested 7 compounds were found to inhibit SDH with IC_{50} values in the micro molar range. Similar studies performed on the much more investigated aldose reductase, the first enzyme of the polyol pathway, have resulted in a similar success rate [17].

Table 1. IC_{50} Values, Molecular Formulae and Chemical Structures of SDI-158 and the Seven SDH Inhibitors Identified from the NCI Database

Compound	Molecular Formula	IC_{50} (μM)	Structure
SDI-158	$C_{11}H_{17}N_5O_3$	1	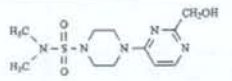
Flavin adenine dinucleotide disodium hydrate	$C_{27}H_{33}N_9O_{15}P_2$	0.19	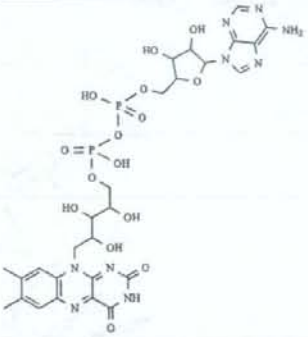
(+)-Amethopterin	$C_{20}H_{22}N_8O_5$	1.1	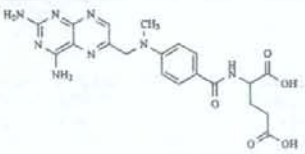
3-Hydroxy-2-napthoic(2-hydroxybenzylidene) hydrazide	$C_{18}H_{14}N_2O_3$	1.2	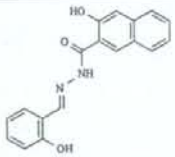
Folic acid	$C_{19}H_{19}N_7O_6$	4.5	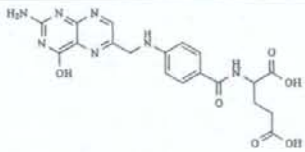
N-2,4-Dinitrophenyl-L-cysteic acid	$C_9H_{10}N_3NaO_9S$	5.3	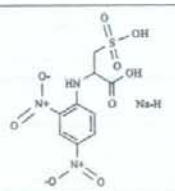

(Table 1. Contd....)

Compound	Molecular Formula	IC_{50} (μM)	Structure
Vanillin azine	$C_{16}H_{16}N_2O_4$	7	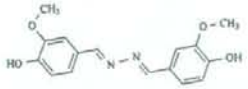
1H-Indole-2,3-dione,5-bromo-6-nitro-1-(2,3,4-tri-O-acetyl-α-L-arabinopyranosyl)-(9CI)	$C_{19}H_{17}BrN_2O_{11}$	28	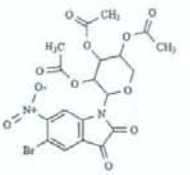

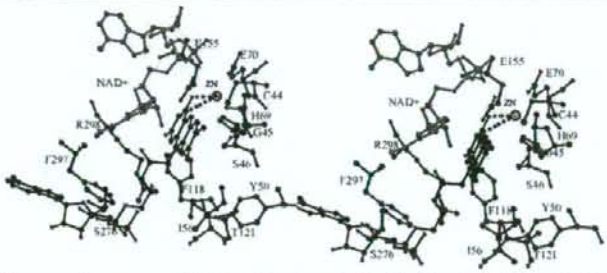

Fig. (1). Stereoview of the most active compound (flavin adenine dinucleotide disodium hydrate) identified from the NCI database and its proposed interactions with the SDH active site. Residues within 4 Å of the compound, H-bonds and the proposed coordination between the zinc atom and the compound (dashed lines) are shown.

REFERENCES

[1] Jedziniak, J.A.; Chylack, L.T.; Cheng, H.-M.; Gillis, M.K.; Kalustian, A.A.; Tung, W.H. *Invest. Ophthalmol. Visual Sci.*, **1981**, *20*, 314.

[2] Ohkubo, Y.; Kishikawa, H.; Araki, E.; Miyata, T.; Isami, S.; Motoyoshi, S.; Kojima, Y.; Furuyoshi, N.; Shichiri, M. *Diabetes Res. Clin. Pract.*, **1995**, *28*, 103.

[3] Obrosova, I.G.; Fathallah, L.; Lang, H.J.; Greene, D.A. *Diabetologia*, **1999**, *42*, 1187.

[4] Pauly, T.; Ekstrom, J.; Beebe, D.; Chrunyk, B.; Cunningham, D.; Griffor, M.; Kamath, A.; Lee, E.; Madura, R.; Mcguire, D.; Subashi, T.; Wasilko, D.; Watts, P.; Mylari, B.; Oates, P.; Adams, P.; Rath, V. *Structure*, **2003**, *11*, 1071.

[5] Johansson, K.; El-Ahmad, M.; Kaiser, C.; Jörnvall, H.; Eklund, H.; Höög, J.; Ramaswamy, S. *Chemico-Biol. Interact.*, **2001**, *130*, 351.

[6] Banfield, M.; Salvucci, M.; Baker, E.; Smith, C. *J. Mol. Biol.*, **2001**, *306*, 239.

[7] Eklund, H.; Nordström, B.; Zeppezauer, E.; Söderlund, G.; Ohlsson, I.; Boiwe, T.; Söderberg, B.-O.; Brändén, C.; Åkeson, A. *J. Mol. Biol.*, **1976**, *102*, 27.

Received: 03 October, 2005 Revised: 16 December, 2005 Accepted: 17 December, 2005

[8] Varlet, D.; Fourmaintraux, E.; Depreux, P.; Lesieur, D. *Heterocycles*, **2000**, *53*, 797.

[9] Chu-Moyer, M.; Ballinger, W.E.; Beebe, D.A.; Berger, R. ; Coutcher, J.B.; Day, W.W.; Li, J.; Mylari, B.L.; Oates, P.J.; Weekly, R.M. *J. Med. Chem.*, **2002**, *45*, 511.

[10] Mylari, B.L.; Oates, P.J.; Zembrowski, W.J.; Beebe, D.A.; Conn, E.L.; Coutcher, J.B.; Linhares, M.C.; Withbroe, G.J. *J. Med. Chem.*, **2002**, *45*, 4398.

[11] Schoichet, B; Bodian, D; Kuntz, I. *J. Comp. Chem.*, **1992**, *13*, 380.

[12] Meng, E.C.; Shoichet, B.K.; Kuntz, I.D. *J. Comput. Chem.*, **1992**, *13*, 505.

[13] Shoichet, B.K.; Kuntz, I.D. *J. Mol. Biol.*, **1991**, *221*, 327.

[14] Mine, G.W.A.; Nicklaus, M.C; Driscoll, J.S.; Wang, S.; Zaharatiz, D. *J. Chem. Inf. Comput. Sci.*, **1994**, *34*, 1219.

[15] Iwata, T.; Popescu, N.C.; Zimonjic, D.B.; Karlsson, C.; Höög, J.-O.; Vaca, G.; Rodriguez, I.R.; Carper, D. *Genomics*, **1995**, *26*, 55.

[16] Darmanin, C.; Iwata, T.; Carper, D.A.; Sparrow, L.G.; Chung, R.P.-T.; El-Kabbani, O. *Acta Cryst.*, **2002**, *D58*, 1379.

[17] Iwata, Y.; Arisawa, M.; Hamada, R.; Kita, Y.; Mizutani, M.Y.; Tomioka, N.; Itai, A.; Miyamoto, S. *J. Med. Chem.*, **2001**, *44*, 1718.

[18] Kraulis, P.J. *J. Appl. Cryst.*, **1991**, *24*, 946.

Involvement of Insulin-like Growth Factor-I and Insulin-like Growth Factor Binding Protein-3 in Corneal Fibroblasts during Corneal Wound Healing

Kanako Izumi,[1,2] Daijiro Kurosaka,[1] Takeshi Iwata,[2] Yoshihisa Oguchi,[1] Yasuhiko Tanaka,[2] Yukihiko Mashima,[1] and Kazuo Tsubota[1]

Purpose. The involvement of downstream messengers of transforming growth factor (TGF)-β in the differentiation of corneal fibroblasts into myofibroblasts was investigated. The effects of insulin-like growth factor (IGF)-I and insulin-like growth factor binding protein (IGFBP)-3 upregulated by TGF-β were examined in human corneal fibroblasts, and the possible involvement of IGF axis components in corneal wound healing was assessed in a mouse model.

Methods. Human corneal fibroblasts were incubated with TGF-β2 or IGF-I, to investigate IGF-I, IGF-II, IGFBP-3, type I collagen, and α-smooth muscle actin (α-SMA) mRNA, as well as IGFBP-3 protein expression, during myofibroblast differentiation. DNA synthesis was evaluated with a 5-bromo-2′-deoxyuridine (BrdU) incorporation assay. IGFBP-3 mRNA expression, protein expression, and immunolocalization were investigated in mouse corneas after photorefractive keratectomy (PRK).

Results. TGF-β2 treatment induced expression of IGF-I and IGFBP-3 mRNA and of IGFBP-3 protein in human corneal fibroblasts. TGF-β2 and IGF-I both stimulated expression of type I collagen. TGF-β2 but not IGF-I potently stimulated α-SMA mRNA expression. IGF-I potently stimulated basal DNA synthesis, whereas IGFBP-3 inhibited it. IGF-I potently stimulated proliferation of TGF-β2-activated myofibroblasts without reversing the activated fibrogenic phenotype, whereas IGFBP-3 suppressed IGF-I-induced proliferation of corneal fibroblasts. IGFBP-3 mRNA and protein increased in mouse corneas soon after PRK, when in vivo immunostaining of the corneas showed expression of IGFBP-3 in the deep layer of the corneal stroma.

Conclusions. These results suggest that during corneal wound healing, TGF-β stimulates IGF axis components, whereas IGFBP-3 may modulate IGF-I-induced myofibroblast proliferation to suppress corneal mesenchymal overgrowth. (*Invest Ophthalmol Vis Sci.* 2006;47:591–598) DOI:10.1167/iovs.05-0097

During corneal wound healing leading to scar formation, keratocytes are activated, turn into fibroblasts, and eventually transformed to α-smooth muscle actin (α-SMA)–expressing myofibroblasts.[1–5] Myofibroblasts are central to wound healing, as they generate the contractile forces necessary for wound closure.[4,6,7] However, regulation of myofibroblast differentiation and proliferation is crucial, because an excessive number of myofibroblasts results in excessive scar formation.[8] Soluble mediators of wound repair, such as growth factors, are important in regulating myofibroblast differentiation and proliferation.

The differentiation of keratocyte into myofibroblasts has been shown to be induced by TGF-β.[3–5,9] TGF-β isoforms regulate multiple biological processes including cell proliferation, extracellular matrix synthesis, angiogenesis, immune response, apoptosis, and differentiation.[7,10–12] They have been implicated in the pathogenesis of fibrosis, autoimmune diseases, cancer, and other disorders.[7,10–12] TGF-β is a pluripotent cytokine capable of inhibiting or stimulating cell growth, depending on the nature of the target cell.[13] TGF-β is a potent inhibitor of growth in a variety of epithelial cell types, whereas in stromal cells it stimulates cell growth.[12,13]

Growth-promoting and metabolic regulatory activities of insulin-like growth factor (IGF)-I and -II are modulated by a family of six high-affinity insulin-like growth factor binding proteins (IGFBPs) and mediated by two IGF receptors (IGF-IR and -IIR), particularly IGF-IR.[14–16] Modulation of IGF actions by IGFBP may be positive or negative, depending on tissue type and physiologic or pathologic states.[15,17–20]

IGFBP-3 is one of the six IGFBPs that regulate binding of IGF-I with the cognate IGF-I receptor tyrosine kinase.[20–23] By modulating the binding of IGF-I to its receptor, an individual IGFBP can either inhibit or augment IGF-I-stimulated growth.[21,24–27] IGFBP-3 is a 40- to 45-kDa glycoprotein produced locally in many tissues, where it serves important paracrine and autocrine functions in modulating cellular growth and apoptosis.[22,25,28] IGFBP-3 activity at the cellular level is regulated, not only by its rate of synthesis, but also by post-translational modification and proteolysis.[29] Several IGFBP-3 proteases have been identified, including plasmin, matrix metalloproteases, kallikreins, prostate-specific antigen, and cathepsin D. This proteolysis results in IGFBP-3 fragments with a low affinity for IGFs.[30,31] IGFBP-3, like IGFBP-1 and IGFBP-5, is capable of regulating cell growth independent of its effects on IGF-I-stimulated growth.[32] For example, IGFBP-3 inhibits replication and promotes apoptosis in various cell lines in an IGF-independent manner.[32] Not only IGF-I but TGF-β1 and TGF-β2 enhance IGFBP-3 mRNA and protein expression in both epithelial and stromal cell types.[33–35] The IGF system plays an important role in wound healing,[14,15] and both IGF-I and IGFBP-3 are present in wound fluid in significant concentrations.[14,15,19]

To our knowledge, the IGFBP-3 system has not been investigated in corneal wound healing. To test our hypothesis that IGF axis components regulate corneal scar formation, we investigated whether TGF-β2 induces IGF-I and IGFBP-3 expression and whether IGFBP-3 modulates IGF-I-induced myofibroblast proliferation in cultured corneal fibroblasts. We then evaluated expression and localization of IGFBP-3 in mouse cornea after photorefractive keratectomy (PRK).

From the [1]Department of Ophthalmology, Keio University School of Medicine, Tokyo, Japan; and the [2]National Institute of Sensory Organs, National Hospital Organization Tokyo Medical Center, Tokyo, Japan.

Submitted for publication January 26, 2005; revised June 29, 2005; accepted December 22, 2005.

Disclosure: **K. Izumi**, None; **D. Kurosaka**, None; **T. Iwata**, None; **Y. Oguchi**, None; **Y. Tanaka**, None; **Y. Mashima**, None; **K. Tsubota**, None

Corresponding author: Daijiro Kurosaka, Department of Ophthalmology, Keio University School of Medicine, 35-Shinanomachi, Shinjuku-ku, Tokyo, 160-8582, Japan; kurosaka@sc.itc.keio.ac.jp.

Materials and Methods

Cell Culture

Human corneal fibroblasts were isolated from corneal limbal rims donated by the Northwest Lions Eye Bank (Seattle, WA). Procedures used in this human-cell in vitro research conformed to the tenets of the Declaration of Helsinki. Corneal tissue was cut into pieces and incubated in a humidified atmosphere of 5% CO_2 and 95% air at 37°C in Dulbecco's modified Eagle's medium (DMEM; Invitrogen-Gibco, Grand Island, NY) containing 10% fetal bovine serum (FBS; Invitrogen-Gibco). Cells in the third passage were used for experiments. The purity of cell cultures was assessed by determining the reactivity with antibodies to vimentin by immunofluorescence analysis. All fibroblasts were immunoreactive for vimentin but not for cytokeratin, suggesting the absence of contamination by epithelial cells.

For reverse-transcription polymerase chain reaction (RT-PCR) experiments, human corneal fibroblasts were cultured at a density of 6.0×10^4/mL in serum-free medium. After 24 hours, this medium was replaced with serum-free medium containing TGF-β2 (0.01–100 ng/mL; R&D Systems, Minneapolis, MN), IGF-I (50 ng/mL; R&D Systems), and anti-IGF-I neutralizing antibody (20 μg/mL; R&D Systems). Incubation was continued for 12, 24, 48, or 72 hours before RNA was extracted for analysis.

For Western blot analysis, human corneal fibroblasts were cultured at a density of 6.0×10^4/mL in serum-free medium. After 24 hours, this medium was replaced with serum-free medium containing 1 ng/mL TGF-β2 for incubations continuing a further 12, 24, 48, or 72 hours before collection of medium for analysis. The conditioned medium was collected, centrifuged to remove cell debris, and stored at −80°C until use.

Photorefractive Keratectomy

Animal procedures were performed in accordance with the ARVO Statement for the Use of Animals in Ophthalmic and Vision Research. Six- to 8-week-old mice (C57BL/6) were used. To induce corneal wounds, first we anesthetized mice by an intraperitoneal injection of 10% pentobarbital (0.15 mg/10 g body weight). A drop of proparacaine HCl (0.05%) was applied to the eye, and the cornea was centered under the laser microscope. Two-millimeter corneal wounds were produced in the right eye of each animal by transepithelial excimer laser abrasion (2-mm optical zone; 42- to 44-μm ablation depth; PTK mode; model EC5000; Nidek, Yokohama, Japan). After excimer laser treatment, tobramycin ointment (0.3%) was applied to the corneal surface to prevent infection. No postoperative topical steroid was administered. At 12 hours and 1, 3, 7, and 14 days after excimer laser ablation, mice were euthanatized for excision of corneas under an operating microscope, these were stored at −80°C until analysis. Thirteen mice were euthanatized at each time point. Five mice at each time point were used for RNA analysis, five for Western blot analysis, and three for immunohistochemistry. Eight corneas from four mice that did not undergo excimer ablation were used as the normal control (day 0).

RNA Extraction

Total RNA was extracted from pooled corneas or cultured fibroblasts after various experimental manipulations. Homogenization was performed in extraction reagent (TRIzol; Invitrogen). Total RNA was extracted from each sample by chloroform, precipitated with isopropanol, and washed with ethanol. RNA pellets were dissolved in diethylpyrocarbonate (DEPC)-treated water and stored at −80°C. The total RNA concentration was measured spectrophotometrically at 260 nm.

PCR Procedure

First-strand cDNA was synthesized with reverse transcriptase (SuperScript II; Invitrogen) and random primer, together with 1 μg of total RNA from the sample. For RT-PCR, gene-specific primers were designed by computer (Primer Express software; Applied Biosystems, Inc., [ABI] Foster City, CA) on the basis of full-length cDNA sequence data (provided by Celera Discovery Systems; ABI). These were as follows: for human IGFBP-3, 5′-CCCAACTGTGACAAGAAGGGATT-3′ (forward primer) and 5′-CAGGCGTCTACTTGCTCTGCAT-3′ (reverse primer); for mouse IGFBP-3, 5′-CCATCCACTCCAT GCCAAGA-3′ (forward primer) and 5′-GGGACTCAGCACATTGAGGAA-3′ (reverse primer); for human IGF-I, 5′-CACCATGTCCTCCTCGCATCT-3′ (forward primer) and 5′-ATCCACGATGCTGTCTGAGG-3′ (reverse primer); for human IGF-II, 5′-CCTGGAGACGTACTGTGCTACC-3′ (forward primer) and 5′-GCTCACTTCCGATTGCTGG-3′ (reverse primer); for human procollagen-α1(I), 5′-AGTCACCCACCGACCAAGAAA-3′ (forward primer) and 5′-CATAAGACAGCTGGGGAGCAAA-3′ (reverse primer); for human α-SMA, 5′-CCAACTGGGACGACATGGAAA-3′ (forward primer) and 5′-GCGTCCAGAGGCATAGAGAGACA-3′ (reverse primer); for human GAPDH, 5′-CAGCCTCAAG ATCATCAGCAAT-3′ (forward primer) and 5′-GGTCATGAGTCCTTCCACGATAC-3′(reverse primer); and for mouse 18S 5′-GATCGAAGACGATCAGATACC-3′ (forward primer) and 5′-CCAGA CAAATCACTCCACC-3′ (reverse primer). The last two of these were used as the endogenous control. Real-time quantitative PCR was performed with a commercial system (model 5000; ABI). Volumes of 50 μL were used for reactions in 96-well plates. The amplification protocol specified incubation at 50°C for 2 minutes and at 95°C for 10 minutes, followed by 40 cycles at 95°C for 15 seconds and 60°C for 1 minute. The PCR cycle number (C_T) at which fluorescence emission reached a threshold value above baseline emission was used to quantitate the original amount of each mRNA, which was normalized to the amount of human GAPDH or mouse 18S.

IGFBP-3 Immunohistochemistry in Mouse Corneal Sections

Eyes harvested at each time point were incubated in 4% paraformaldehyde and phosphate-buffered saline (PBS) overnight at 4°C. Paraffin-embedded sections were cut at a 4-μm thickness and affixed to glass slides (Superfrost; Matsunami, Osaka, Japan). Formalin-fixed paraffin-embedded sections of tissue were heated, dewaxed, and rehydrated before blocking of endogenous peroxidase (0.1%, vol/vol hydrogen peroxide). Sections were incubated with polyclonal rabbit antibody against mouse IGFBP-3 (GroPep, Adelaide, Australia). Specific binding was detected by an Alexa 488-conjugated anti-rabbit secondary antibody (Molecular Probes, Eugene, OR). The sections were counterstained with propidium iodine, and mounted in anti-fading solution (Vector Laboratories, Burlingame, CA). In addition to the fluorescent conjugate, primary antibody was detected with an immunoperoxidase protocol (Envision kit; Dako, Ely, UK). Fluorescent images were photographed with a laser scanning confocal microscope (LSM510; Carl Zeiss Meditec, Jena, Germany).

Western Blot Analysis

For Western blot analysis, 10 mL serum-free conditioned medium collected from each flask was concentrated by centrifugation in a spin column (Centricon 50; Millipore, Bedford, MA) to achieve a 200-fold concentration. Protein from the concentrated conditioned medium of corneal fibroblasts or protein extracted from mouse cornea after PRK was analyzed for IGFBP-3 on 15% SDS-polyacrylamide gels and then electrophoretically transferred to polyvinylidene difluoride (PVDF) membrane. Overall protein concentrations were determined by the Lowry assay. Transfer was performed at a constant voltage of 60 V for 1 hour. After transfer, the membrane was incubated in Tris-buffered saline (TBS) containing 5% skim milk for 1 hour at room temperature. The membrane was rinsed three times with TBS-0.1% Tween, and then incubated with an anti-human IGFBP-3 monoclonal antibody (R&D Systems) or a polyclonal rabbit antibody against mouse IGFBP-3 (GroPep) for 2 hours at room temperature. The membrane was rinsed with TBS-0.1% Tween and then incubated with horseradish peroxidase-labeled goat anti-rabbit IgG (Jackson ImmunoResearch Laborato-

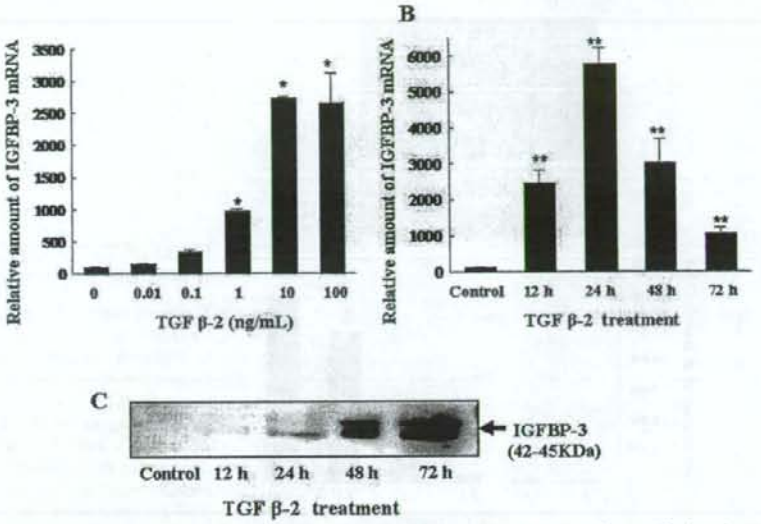

FIGURE 1. TGF-β2 stimulation of IGFBP-3 production by corneal fibroblasts. (A) IGFBP-3 mRNA expression in the presence of various concentrations of TGF-β2. Corneal fibroblasts were incubated for 24 hours in serum-free medium in the absence or presence of TGF-β2 at concentrations ranging from 0.01 to 100 ng/mL. The relative amount of IGFBP-3 mRNA compared with that in the untreated control was determined by real-time quantitative PCR. *Significantly different ($P < 0.05$) from the serum-free control. (B) Time course of IGFBP-3 mRNA expression in corneal fibroblasts after treatment with 1 ng/mL TGF-β2. The relative amount of IGFBP-3 mRNA compared with the untreated control was determined by real-time quantitative PCR. **Significantly different ($P < 0.05$) from 0-hour control. (C) Western blot of conditioned medium, performed to determine the time course of IGFBP-3 secretion from corneal fibroblasts. Media from untreated cells or cells treated for 12, 24, 48, or 72 hours with 1 ng/mL TGF-β2 were concentrated and subjected to immunoblot analysis with an antibody against IGFBP-3. Data are representative of results in three independent experiments.

ries, West Grove, PA) for 1 hour at room temperature. The membrane then was rinsed thoroughly with TBS-0.1% Tween. Bound antibody was detected with a chemiluminescence detection kit (Super Signal West Femto Maximum Sensitivity Substrate; Pierce Biotechnology, Rockford, IL) and an imager (Lumi Imager; Roche Diagnostics, Mannheim, Germany).

Assays of DNA Synthesis

The effect of TGF-β2, IGF-I, and IGFBP-3 on corneal fibroblast proliferation was assessed by BrdU incorporation using a BrdU enzyme-linked immunosorbent assay (ELISA; Cell Proliferation ELISA, BrdU colorimetric; Roche Diagnostics) according to the instructions of the manufacturer. Corneal fibroblasts were cultured in 96-well plates (2.8×10^3 per well) for 24 hours in DMEM containing 0.1% bovine serum albumin (BSA), after which the culture medium was further supplemented with growth factors. Control cultures were incubated in the absence of growth factor. To study the effect of exogenous TGF-β2, IGF-I, and IGFBP-3 on DNA synthesis, we incubated corneal fibroblasts for 24 hours in the presence of TGF-β2 (0.01–10 ng/mL), IGF-I (50 ng/mL), IGFBP-3 (50–1000 ng/mL), and immunoneutralizing antibody against IGFBP-3 (10 μg/mL; R&D Systems). Cells were pulse labeled for 24 hours with 100 μM BrdU. All assays were performed in triplicate or quadruplicate and were replicated in at least two separate experiments.

Statistical Analysis

Data are presented as the mean ± SD and were analyzed by one-way analysis of variance (ANOVA). Post hoc comparisons between groups used the Fisher protected least significant difference test. $P < 0.05$ was accepted as indicating statistical significance. All experiments in this study were repeated at least three times, in the same conditions.

RESULTS

Induction of IGFBP-3 Expression by TGF-β2 in Human Corneal Fibroblasts

We began the present study by asking whether TGF-β2-treated human corneal fibroblasts express IGFBP-3 at the mRNA and protein levels, using real-time quantitative PCR and Western blot analysis. Figure 1A shows that treatment with TGF-β2 significantly stimulated the expression of endogenous IGFBP-3 in a TGF-β2 dose-dependent manner (Fig. 1B). As for time, 1 ng/mL TGF-β2 increased IGFBP-3 protein production within 24 hours of addition (Fig. 1C), after 72 hours, the degree of stimulation was much greater.

Effect of IGFBP-3 on DNA Synthesis by Corneal Fibroblasts

We next asked how IGFBP-3 affects corneal fibroblast DNA synthesis. Addition of IGFBP-3 to corneal fibroblasts significantly inhibited basal DNA synthesis in a dose-dependent man-

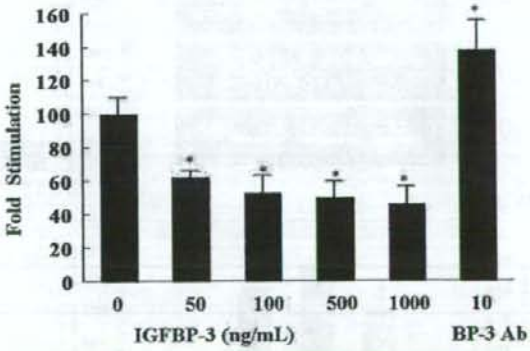

FIGURE 2. Effect of IGFBP-3 on DNA synthesis in human corneal fibroblasts. Cells were cultured for 24 hours in DMEM containing 0.1% BSA in the absence or presence of IGFBP-3 at concentrations ranging from 50 to 1000 ng/mL, or in the presence of 10 μg/mL IGFBP-3 neutralization antibody (BP-3 Ab). Cells were pulse-labeled with BrdU for 24 hours. Data represent the mean ± SD of results in three experiments, in which determinations were performed in triplicate. *Significantly different ($P < 0.05$) from the serum-free control.

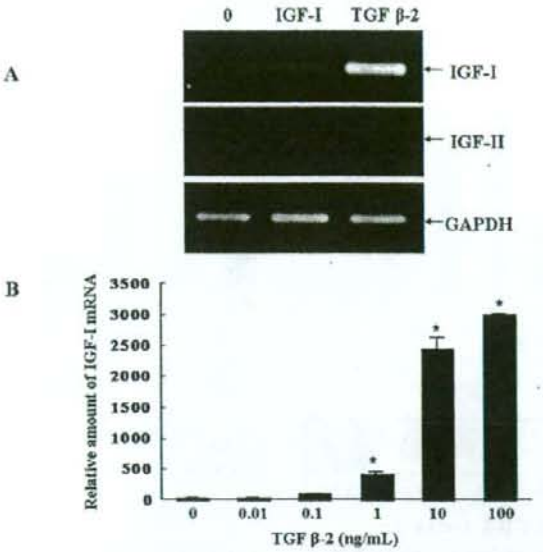

FIGURE 3. IGF-I and IGF-II mRNA expression in response to TGF-β2 (1 ng/mL) and IGF-I (50 ng/mL). (**A**) Ethidium bromide-stained agarose gels show PCR products for IGF-I and -II amplified from reverse-transcribed RNA isolated from human corneal fibroblasts treated with TGF-β2 or IGF-I for 24 hours. Note the induction of IGF-I, but not IGF-II, by TGF-β2. This experiment was replicated three times. (**B**) IGF-I mRNA expression in response to various concentrations of TGF-β2. The relative amount of IGF-I mRNA compared with that in the untreated control was determined by real-time quantitative PCR. *Significantly different ($P < 0.05$) from the serum-free control.

ner (Fig. 2), whereas basal DNA synthesis in corneal fibroblasts was increased in the presence of the IGFBP-3-neutralizing antibody. The result implied that endogenous IGFBP-3 directly inhibits corneal fibroblast proliferation.

Induction of IGF mRNA Expression by TGF-β2 in Human Corneal Fibroblasts

Next, we investigated the effect of TGF-β2 on expression of other components of the IGF axis. RT-PCR was used to determine whether mRNA expression of IGFs is altered by TGF-β2. Treatment with TGF-β2 stimulated expression of endogenous IGF-I mRNA but not that of IGF-II mRNA (Fig. 3A). As shown in Figure 3B, TGF-β2 induced IGF-I expression in a dose-dependent manner.

Effect of TGF-β2 and IGF-I on Type I Collagen and α-SMA mRNA Expression

We next assessed the effect of IGF-I and TGF-β2 on type I collagen and α-smooth muscle actin expression. As shown in Figure 4, in cells treated for 48 hours, IGF-I and TGF-β2 induced a similar increase in type I collagen mRNA. Furthermore, corneal fibroblasts treated with TGF-β2 and anti IGF-I neutralizing antibody also induced significant upregulation of COLIA1 mRNA compared with the untreated control. Treatment with TGF-β2 and anti-IGF-I neutralizing antibody significantly suppressed this expression compared with TGF-β2 treatment. In contrast, although TGF-β2 treatment resulted in a fivefold increase in α-SMA mRNA expression, no α-SMA mRNA increase was detected in response to IGF-I.

Effect of TGF-β2 and IGF-I on DNA Synthesis by Corneal Fibroblasts

To determine whether addition of TGF-β2 or IGF-I to corneal fibroblasts affects DNA synthesis, we used a BrdU incorporation assay. As shown in Figure 5, incubation with IGF-I for 24 hours significantly stimulated DNA synthesis in cultured corneal fibroblasts compared with the untreated control. Whereas a low concentration of TGF-β2 enhanced corneal fibroblast DNA synthesis, a high concentration inhibited it.

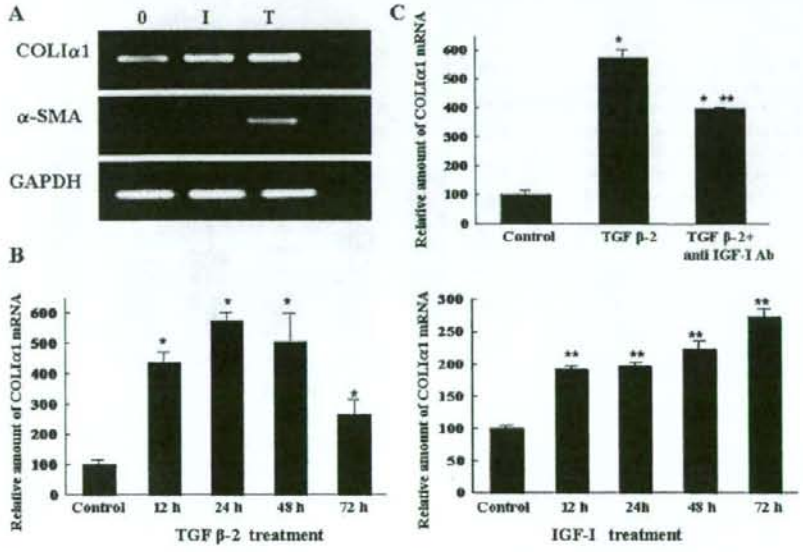

FIGURE 4. Procollagen-Iα1 and α-SMA mRNA expression in response to TGF-β2 and IGF-I. (**A**) Ethidium bromide–stained agarose gels show PCR products for procollagen-Iα1 and α-SMA amplified from reverse-transcribed RNA isolated from human corneal fibroblasts after treatment with TGF-β2 (T) or IGF-I (I) for 24 hours. (**B**) Time course of procollagen-Iα1 mRNA expression in corneal fibroblasts after treatment with TGF-β2 or IGF-I. The relative amount of procollagen-Iα1 mRNA compared with that in the untreated control was determined by real-time quantitative PCR. *Significantly different ($P < 0.05$) from 0-hour control. **Significantly different ($P < 0.05$) from 0-hour control. (**C**) COLIA1 mRNA expression in response to TGF-β2 or TGF-β2+anti-IGF-I neutralizing antibody for 24 hours. The relative amount of COLIA1 mRNA compared with that of the untreated control was determined by real-time quantitative PCR. *Significantly different ($P < 0.05$) from the serum-free control. **Significantly different ($P < 0.05$) from TGF-β2 treatment groups.

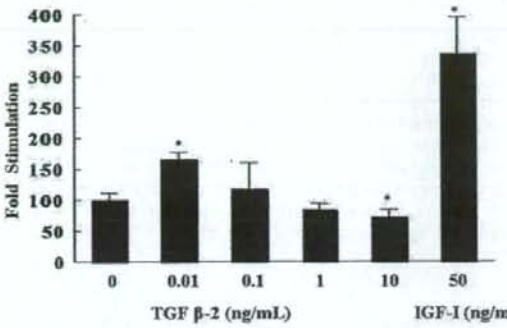

FIGURE 5. Effects of TGF-β2 and IGF-I on DNA synthesis in human corneal fibroblasts. Cells were cultured for 24 hours in DMEM containing 0.1% BSA in the absence or presence of TGF-β2 at concentrations ranging from 0.01 to 10 ng/mL or 50 ng/mL IGF-I. Cells were pulse labeled with BrdU for 24 hours. Data represent the mean ± SD of results in three different experiments performed in triplicate. *Significantly different ($P < 0.05$) from the serum-free control.

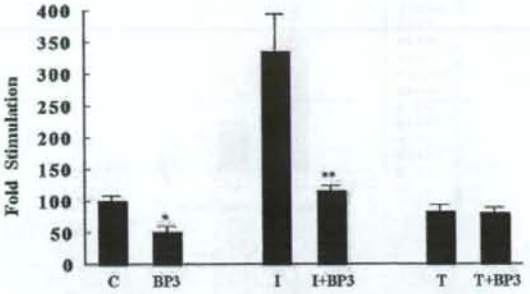

FIGURE 7. IGFBP-3 modulated basal and IGF-I-stimulated DNA synthesis. Human corneal fibroblasts were preincubated with 1000 ng/mL IGFBP-3 (BP3) for 24 hours before addition of medium supplemented with BrdU and 50 ng/mL IGF-I (I) or 1 ng/mL TGF-β2 (T). Data represent the mean ± SD of results in three different experiments performed in triplicate. *Significantly different ($P < 0.05$) from the serum-free control; **Significantly different ($P < 0.05$) from IGF-I-treated cells. C, serum-free control.

Effect of IGF-I on Proliferation and Characteristics of Corneal Myofibroblasts Induced by TGF-β2

We next asked whether TGF-β2 and IGF-I act sequentially in regulating the activated myofibroblast phenotype or cell proliferation. Cells were pretreated with TGF-β2, followed by substitution of medium containing IGF-I but not TGF-β2. Cells pretreated with TGF-β2 for 7 days showed a significant increase in DNA synthesis when subsequently exposed to IGF-I instead (Fig. 6A). To determine whether IGF-I affects the activated phenotype induced by TGF-β2, cells pretreated with TGF-β2 for 7 days were exposed to serum-free medium, without or with IGF-I, for 3 days and then immunostained for α-smooth muscle actin. A large percentage of corneal fibroblasts that expressed α-smooth muscle actin after 7 days of TGF-β2 treatment maintained the expression of α-SMA after exposure for 3 days to serum-free medium or IGF-I. The activated phenotype therefore was not reversed spontaneously or by IGF-I over this time frame (Fig. 6B).

Modulation of Basal and IGF-I-Stimulated DNA Synthesis by IGFBP-3

Interaction between IGFBP-3 and IGF-I or TGF-β2 then was considered in terms of DNA synthesis by corneal fibroblasts. When added to medium together with IGF-I, IGFBP-3 significantly inhibited IGF-I-stimulated DNA synthesis. However, IGFBP-3 did not affect the inhibitory effect of 1 ng/mL TGF-β2 on basal DNA synthesis (Fig. 7) or TGF-β2-stimulated expression of α-SMA and type I collagen (data not shown).

Effect of PRK on IGFBP-3 mRNA and Protein Levels in Mouse Cornea

To investigate the involvement of IGFBP-3 in corneal wound healing in vivo, we studied IGFBP-3 expression in mouse cor-

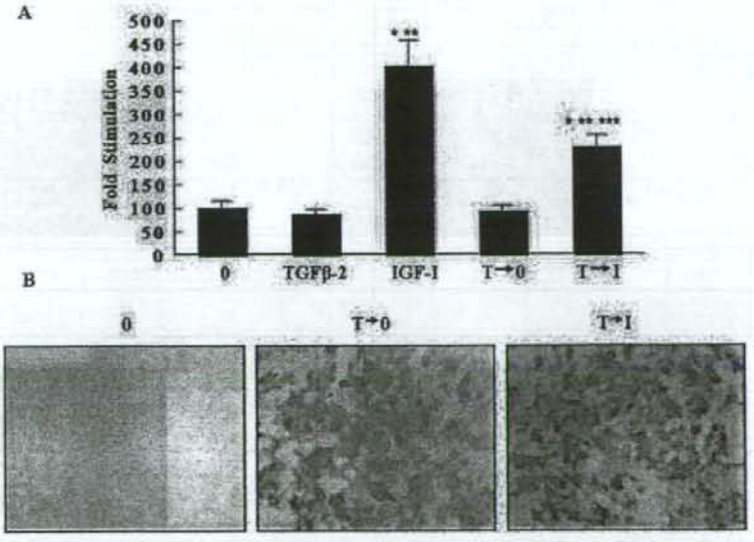

FIGURE 6. Effects of sequential treatment with TGF-β2 and IGF-I. (A) DNA synthesis in response to IGF-I (50 ng/mL) in human corneal fibroblasts pretreated with TGF-β2 (1 ng/mL). After pretreatment for 7 days, TGF-β2 was removed, and serum-free medium supplemented with only BrdU (T→0) or BrdU+IGF-I (T→I) was added for 24 hours. Data represent the means ± SD of results in three experiments performed in triplicate. *Significantly different ($P < 0.05$) from the serum-free control. **Significantly different ($P < 0.05$) from TGF-β2 treatment groups. ***Significantly different ($P < 0.05$) from the T→0 groups. (B) Immunostaining of human corneal fibroblasts with α-SMA-specific antibody after pretreatment with TGF-β2 for 7 days, followed by removal of TGF-β2 and subsequent treatment with serum-free medium (T→0) or IGF-I (T→I) for another 3 days. 0, nonstimulated, negative control. Magnification, ×40.

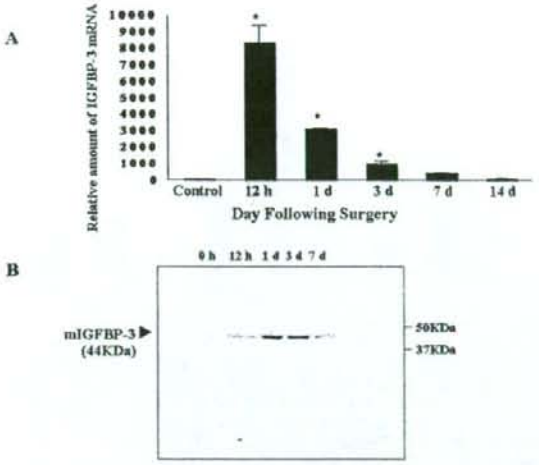

FIGURE 8. Expression of IGFBP-3 in mouse corneas after PRK. (A) The relative amount of IGFBP-3 mRNA compared with control corneas without surgery was determined by real-time quantitative PCR. Six mouse corneas were analyzed for this RNA at 0 or 12 hours, 1 day or 3, 7, or 14 days after PRK. *Significantly different ($P < 0.05$) from the untreated control. (B) Western blot analysis of IGFBP-3 expression in mouse corneas after PRK. Six mouse corneas were analyzed for this protein at 0 or 12 hours or 1 day or 3 or 7 days after PRK.

neas after PRK. As shown in Figure 8, amounts of IGFBP-3 mRNA and protein significantly increased in mouse corneas after PRK. In particular, IGFBP-3 mRNA dramatically increased in the cornea at 12 hours after PRK, compared with control corneas without PRK. IGFBP-3 mRNA then progressively decreased with time. IGFBP-3 protein increased significantly at days 1 and 3 compared with the untreated control corneas, declining to normal by day 7.

IGFBP-3 Localization in Mouse Cornea after PRK

Localization of IGFBP-3 during mouse corneal wound healing after PRK was examined by immunostaining. As shown in Figure 9, IGFBP-3 was immunolocalized in paraffin-embedded sections of mouse corneas harvested at the same time points after surgery at which protein and RNA were measured. IGFBP-3 was detected in only slight amounts in the stromal matrix of normal corneas before PRK (day 0). On day 1 after surgical injury, intense staining was present in the deep layer of the corneal stroma. By day 7, staining in the deep stromal layer was reduced, in agreement with the results of Western blot analysis.

DISCUSSION

IGFBP-3, the major serum transport protein for IGFs, also is active in the cellular environment, where it acts as a potent antiproliferative agent.[22,23,28] We found that in human corneal fibroblasts, TGF-β induced expression of IGFBP-3 mRNA and protein, whereas IGFBP-3 inhibited DNA synthesis in corneal fibroblasts. In addition to its effect on IGFBP-3, TGF-β induced IGF-1 mRNA expression. IGF-I promoted proliferation of myofibroblasts without reversing the activated phenotype. We conclude that during corneal wound healing, IGF axis components are likely to regulate corneal mesenchymal overgrowth and suppress corneal stromal wound contraction.

TGF-β is a well-established mediator of wound healing and fibrosis in several organs.[5,6] In the cornea, it potently activates keratocytes to a myofibroblast phenotype expressing α-SMA and also induces expression of type I collagen.[5–5,9] Previous reports of potent upregulation of IGFBP-3 by TGF-β in subconfluent fibroblasts[34,35] were confirmed in our corneal cells in subconfluent, serum-free culture. In accord with evidence that IGFBP-3 plays a role in antiproliferation,[23,28] IGFBP-3 appeared to suppress proliferation of myofibroblasts induced by TGF-β.

Potentiation and inhibition of IGF action by IGFBP-3 have been demonstrated in many cell culture systems.[17,18,22] It is thought that cotreatment of cells with IGFBP-3 and IGF-I causes

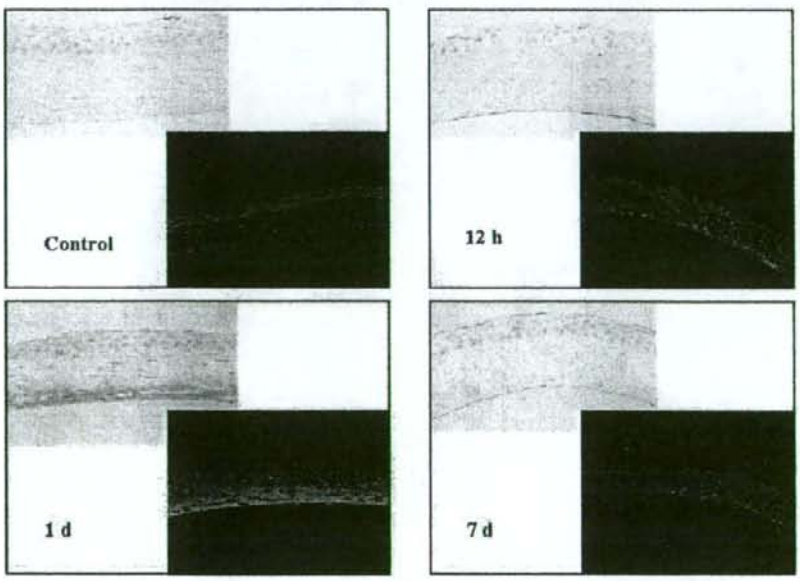

FIGURE 9. Immunolocalization of IGFBP-3 in mouse corneas at 0 or 12 hours or 1 day or 7 days in mouse corneas after PRK. IGFBP-3 was localized using an alkaline phosphatase visualization substrate. Images were obtained from the same field by fluorescence microscopy. Mouse corneas were subjected to immunofluorescent staining with antibodies to IGFBP-3 (*green*) and the nuclear marker propidium iodine (*red*). Magnification, ×200.

IGFBP-3 to inhibit IGF-I-mediated effects via high-affinity sequestration of the ligand, presumably leading to prevention of IGF-I–induced IGF-RI autophosphorylation and signaling.[22,23] In cornea, epithelial cells and fibroblasts express IGF-I, IGF-II, and IGF-IR.[37] IGF-I is suggested to play a critical role in the maintenance of the keratocyte phenotype[38] and has been shown to be mitogenic for human corneal fibroblasts[39] and protective against apoptosis.[40] IGF-I also has been shown to be chemotactic for human corneal fibroblasts,[41] and to enhance epidermal growth factor stimulated collagen gel contraction.[42] The effects of TGF-β on IGF-I and IGFBP-3 mRNA observed in our present experiments have important implications for regulation of corneal mesenchymal overgrowth during corneal wound healing. Our new observations that TGF-β2 induces expression of IGF-I in corneal fibroblasts and that IGF-I stimulates growth of corneal fibroblasts activated to a myofibroblast phenotype by TGF-β2 suggest that such regulation may take place during corneal stromal wound healing. The myofibroblast phenotype was not reversed by IGF-I. Furthermore, our study supports a role for IGF-I, together with TGF-β2, as an upregulator of extracellular matrix (ECM) synthesis during corneal stromal wound healing. IGF-I, then, is critical not only to maintenance of the keratocyte phenotype in intact cornea, but to regulation of myofibroblast behavior in injured cornea. These aspects of IGF-I activity in corneal wound healing currently are being studied in corneal cell culture.

Our findings that TGF-β induced upregulation of IGFBP-3 mRNA by 12 hours after TGF-β treatment and that immunoneutralization of endogenous IGFBP-3 increased basal DNA synthesis in corneal fibroblasts suggest possible IGF-independent effects of IGFBP-3. In several carcinoma cell lines and in some normal cells, IGFBP-3 regulates cell growth independent of IGF-I.[25,43] Two mechanisms for this effect have been identified[23]: The first involves the interaction of IGFBP-3 with TGF-β receptors and TGF-β-dependent signaling mechanisms[23]; the second involves the interaction of IGFBP-3 with nuclear retinoid X receptor-α (RXR-α).[44,45] Furthermore, recent studies have shown that endogenous IGFBP-3 directly inhibits proliferation of human intestinal smooth muscle cells by activation of TGF-βRI and Smad2.[46] Although this IGFBP-3-dependent inhibition of growth is mediated via TGF-β receptors, these effects are independent of endogenous TGF-β because immunoneutralization of endogenous TGF-β does not diminish IGFBP-3-dependent Smad2 activation or IGFBP-3-dependent inhibition of [^{3}H] thymidine incorporation.[46] Therefore, one may postulate that IGFBP-3 also inhibits corneal fibroblast growth directly, helping to prevent excessive proliferation of fibroblasts before their differentiation to the activated phenotype in the wound cornea.

The ability of IGFBP-3 to bind other molecules has been demonstrated previously.[47–49] Recent studies have shown that plasminogen binds IGFBP-3 and the binary IGF-I/IGFBP-3 complex with high affinity by interacting directly with the IGFBP-3 heparin-binding domain.[47] In vitro studies have shown that hypertrophic scar fibroblasts produce elevated levels of IGFBP-3 and type Iα collagen and that TNF-α treatment reduces IGFBP-3 and collagen expression in a dose-dependent fashion.[49] A recent report indicated that physiologic effects of IGFBP-3-collagen interaction may include modulation of cell adhesion and migration because they characterized type Iα collagen as one of the IGFBP-3 binding proteins.[50] In our present in vivo experiments, strong IGFBP-3 immunoreactivity was found in the extracellular matrix of mouse corneal stroma at an early time point during wound healing after PRK. This IGFBP-3 may bind to the collagen matrix and contribute to regulation of corneal stromal wound healing.

After refractive surgery, a corneal subepithelial haze develops in some patients as a wound healing response.[1,2] This reaction has been reported to be associated with increased myofibroblast transformation.[3–6] When it follows PRK, the corneal haze develops in the subepithelial lesion,[1,2] not in the deep stromal layer. We found immunostaining for IGFBP-3 at an early time point after PRK to be much stronger in the deep stromal than subepithelially. IGFBP-3, then, may act to suppress formation of haze by inhibiting the proliferation of corneal myofibroblasts. Pathologic fibrosis and myofibroblast formation induced by TGF-β within the eye represents a significant pathophysiologic problem and may lead, not only to a subepithelial corneal haze, but to various other adverse effects, such as posterior capsular opacification,[51] anterior subcapsular cataract,[52,53] and trabeculectomy bleb failure.[54] As yet, no report has characterized the activity of IGFBP-3 in these conditions. Our study may expand the possibilities for preventing these adverse effects, because IGFBP-3 has hidden potential to become a key factor in various fibroses and wound contraction.

We present evidence of the induction of IGFBP-3 by TGF-β treatment of corneal fibroblasts. We found that the combined actions of TGF-β and IGF-I would stimulate collagen synthesis in healing, whereas proliferation would be limited by IGFBP-3 induced by TGF-β. Persistent expression of IGF-I in cells exposed to TGF-β would permit proliferation of myofibroblasts, resulting in fibrosis. It is noteworthy that the effect of TGF-β2 to induce both IGF-I and IGFBP-3 indicates that, if such an effect occurs in vivo, the spatial and temporal distribution of IGF-I and IGFBP-3 may have major effects on the degree to which fibrogenic populations of myofibroblasts are expanded. The current report demonstrates that IGFBP-3 induced by TGF-β may be critical in the suppression of mesenchymal overgrowth after corneal injury.

References

1. Jester JV, Petroll WM, Cavanagh HD. Corneal stromal wound healing in refractive surgery: the role of myofibroblasts. *Prog Retin Eye Res*. 1999;18:311–356.
2. Fini ME. Keratocyte and fibroblast phenotypes in the repairing cornea. *Prog Retin Eye Res*. 1999;18:529–551.
3. Jester JV, Huang J, Barry-Lane PA, et al. Transforming growth factor (beta)-mediated corneal myofibroblast differentiation requires actin and fibronectin assembly. *Invest Ophthalmol Vis Sci*. 1999;40:1959–1967.
4. Jester JV, Petroll WM, Barry PA, Cavanagh HD. Expression of alpha-smooth muscle (alpha-SM) actin during corneal stromal wound healing. *Invest Ophthalmol Vis Sci*. 1995;36:809–819.
5. Jester JV, Barry-Lane PA, Cavanagh HD, Petroll WM. Induction of alpha-smooth muscle actin expression and myofibroblast transformation in cultured corneal keratocytes. *Cornea*. 1996;15:505–516.
6. Garana R, Petroll W, Chen WT, et al. Radial keratotomy: role of myofibroblasts in corneal wound contraction. *Invest Ophthalmol Vis Sci*. 1992;33:3271–3281.
7. Friedman SL. Molecular regulation of hepatic fibrosis, an integrated cellular response to tissue injury. *J Biol Chem*. 2000;275:2247–2250.
8. Nedelec B, Ghahary A, Scott PG, Tredget EE. Control of wound contraction: basic and clinical features. *Hand Clin*. 2000;16:289–302.
9. Kurosaka H, Kurosaka D, Kato K, Mashima Y, Tanaka Y. Transforming growth factor-beta 1 promotes contraction of collagen gel by bovine corneal fibroblasts through differentiation of myofibroblasts. *Invest Ophthalmol Vis Sci*. 1998;39:699–704.
10. Desmouliere A, Gabbiani G. Myofibroblast differentiation during fibrosis. *Exp Nephrol*. 1995;3:134–139.
11. Li H, He B, Que C, Weng B. Expression of TGF-beta 1, PDGF and IGF-I mRNA in lung of bleomycine-A5-induced pulmonary fibrosis in rats. *Chin Med J*. 1996;109:533–536.